JOURNAL OF GEOPHYSICAL RESEARCH, VOL. 92, NO. A6, PAGES 5768–5776, JUNE 1, 1987

Electron Cyclotron Harmonic Waves Observed by the AMPTE-IRM Plasma Wave Experiment Following a Lithium Release in the Solar Wind

J. L. ROEDER,[1] H. C. KOONS,[1] R. H. HOLZWORTH,[2] R. R. ANDERSON,[3] O. H. BAUER,[4] D. A. GURNETT,[3] G. HAERENDEL,[4] B. HÄUSLER,[4] AND R. TREUMANN[4]

An unexpected occurrence following the second lithium release by the AMPTE-IRM spacecraft in the solar wind on September 20, 1984, was the appearance of electron cyclotron harmonic emissions. These emissions began about 50 s after the release and continued for several minutes. Narrow-band emissions polarized perpendicular to the magnetic field with amplitudes of approximately 10^{-5} V m^{-1} were observed in each of the first five harmonic bands. Unpolarized diffuse emissions were also present at the same time. The diffuse emissions extended from below the lowest measured frequency channel to above the highest narrow-band emission with a maximum below the electron cyclotron frequency. It will be shown that these observations are inconsistent with their generation by several ion beam instabilities.

INTRODUCTION

The Active Magnetospheric Particle Tracer Explorers (AMPTE) program performed two lithium releases in the solar wind upstream of the earth's bow shock in September 1984. These events were presented in some detail in earlier papers [*Lühr et al.*, 1986; *Paschmann et al.*, 1986; *Häusler et al.*, 1986; *Gurnett et al.*, 1986; *Coates et al.*, 1986; *Hall et al.*, 1986; *Möbius et al.*, 1986]. An unpredicted occurrence following the second lithium release was the appearance of electrostatic emissions near the harmonics of the electron cyclotron frequency [*Häusler et al.*, 1986]. Similar harmonic waves were not observed during the first AMPTE lithium release. The observations, analysis, and interpretation of these emissions are presented in this paper.

The AMPTE program is a series of active experiments with two purposes: to study the access of solar wind ions to the magnetosphere and to investigate the physics of the interaction of an injected plasma cloud with an existing cosmical plasma [*Krimigis et al.*, 1982; *Bryant et al.*, 1985]. Three spacecraft are involved in the AMPTE project: the Ion Release Module (IRM), which releases the chemical canisters, the United Kingdom Subsatellite (UKS), which orbits near the IRM to study the expansion and evolution of the releases, and the Charge Composition Explorer (CCE), which searches for the tracer ions in the inner regions of the magnetosphere. The data presented in this paper were obtained from the plasma diagnostic instruments aboard the IRM. During the September 1984 releases the IRM was at apogee on the dayside of the earth near local noon.

[1]Space Sciences Laboratory, The Aerospace Corporation, Los Angeles, California.
[2]Space Sciences Division, University of Washington, Seattle.
[3]Department of Physics and Astronomy, University of Iowa, Iowa City.
[4]Max Planck Institute for Physics and Astrophysics, Institute for Extraterrestrial Physics, Garching by Munich, Federal Republic of Germany.

Paper number 6A8375.
0148-0227/87/006A-8375$05.00

INSTRUMENTATION

The electric and magnetic field emissions described in this paper were measured by the IRM plasma wave instrument described in detail by *Häusler et al.* [1985]. This instrument uses a 47-m tip-to-tip electric dipole antenna for electric field measurements and two search coil antennas for low-frequency and high-frequency magnetic field measurements. The signals from the antennas were processed by a variety of on-board spectrum analyzers covering the frequency range 31 Hz to 5.6 MHz. These included a stepped frequency receiver (SFR), which is a 96-channel spectrum analyzer from 200 Hz to 100 kHz with a temporal resolution of 1 s. The ac electric field was also telemetered to the ground via two wideband analog channels equipped with automatic gain control (AGC) systems. These channels have bandwidths from 650 Hz to 10 kHz and from 5 Hz to 1 kHz, respectively. The sensitivity of the electric field measurement is approximately 5×10^{-8} V m^{-1} Hz$^{-1/2}$ in the frequency range 0.2–2.6 kHz. The sensitivity of the magnetic data channel is set by the spacecraft noise level, which is approximately 10^{-5} gamma Hz$^{-1/2}$.

WAVE OBSERVATIONS

The lithium was released into the solar wind for the first time at 0756 UT on September 11, 1984, and for the second time at 0956 UT on September 20, 1984. A detailed description of the wave phenomena observed during these two experiments is given by *Häusler et al.* [1986]. The interplanetary conditions at the times of the releases were quite different, as presented in Table 1, taken from *Häusler et al.* [1986]. During the first release the solar wind velocity was very high (700 km/s), and the direction of the magnetic field was approximately parallel to the flow direction of the solar wind. Most of the field and plasma quantities were highly variable on time scales of 1–60 s due to the presence of particles reflected upstream from the earth's bow shock. The second release occurred during a more "normal" case with the magnetic field approximately perpendicular to flow velocity. The lack of upstream events on September 20 resulted in a much quieter plasma environment for the active experiment. The IRM observed identifiable electron cyclo-

TABLE 1. Interplanetary Conditions

	Release 1	Release 2
n, cm^{-3}	1–4	4–10
V_{sw}, km/s	680	460
ϕ_V, deg	171.5	175.0
θ_V, deg	+3	+4
B, nT	6	8
ϕ_B, deg	4.0	120.0
θ_B, deg	−10	+15

tron harmonic emissions only in connection with the second release.

Almost immediately after each of the releases a diamagnetic cavity was formed around the IRM spacecraft. During the second release the cavity was observed for approximately 7 s, as described by *Lühr et al.* [1986]. After the cavity was convected downstream by the solar wind, the magnetic field returned to the prerelease value in approximately 40 s. The electron cyclotron harmonic emissions were observed by the IRM during the 3 min following the magnetic field recovery.

A spectrogram of 15 min of data from the SFR is shown in Plate 1. The spectrogram is partitioned into three panels, each of which displays the data from a 32-channel analyzer producing one spectrum per second. The bottom panel shows the magnetic data in the frequency range 0.2–2.5 kHz, the middle panel shows the electric data in a similar frequency range, and the top panel shows the electric data from 9 to 99 kHz. The linear frequency scales are marked on the left side of the figure. The data are color coded according to the scale on the right side of the figure. The horizontal reddish lines at the bottom of each panel are calibration signals and represent approximately the largest amplitude allowable for each analyzer. The abscissa is marked with the universal time, the spacecraft geocentric distance in earth radii, and the local time in hours.

The spiked feature in the middle panel is a 10-s interval of very intense electric noise which began 17 s after the injection. This emission has been interpreted as the result of an ion beam–plasma instability within a shocklike structure near the upstream edge of the magnetic cavity [*Gurnett et al.*, 1986]. At approximately 0956:30 UT there began a diffuse emission at frequencies from less than 5 Hz to approximately 400 Hz. The upper cutoff frequency of these emissions increased at 0956:55 UT to approximately 2.5 kHz. Superimposed on the spectrum of the diffuse emissions were enhancements at frequency intervals near the electron cyclotron frequency. During the time interval when these waves were observed, the measured magnetic field remained at 8.9 ± 0.3 gammas, corresponding to an electron cyclotron frequency of 249 ± 8 Hz. These electron cyclotron harmonic (ECH) emissions and diffuse emissions continued for several minutes, with a decreasing upper cutoff frequency, as shown by the triangular region in the middle panel in Plate 1. They are identified by the faint horizontal banding, which attained levels of 2×10^{-6} V m^{-1} Hz$^{-1/2}$. The absence of any magnetic signal in the bottom panel which is identifiable with the electric emission limits the magnetic component of the waves to less than 10^{-5} gamma Hz$^{-1/2}$. The horizontal lines in the magnetic spectrogram are spacecraft interference. These field magnitudes correspond to an index of refraction of the order of unity, which is a value consistent with that of electromagnetic waves. Therefore the magnetic measurement can provide no information regarding the magnetic component of the emissions. As shown below, the emissions may be assumed to be electrostatic on the basis of spectral and polarization measurements.

The line emission in the top panel of Plate 1 at a frequency of 25 kHz is interpreted as a Langmuir emission at the local electron plasma frequency. This frequency corresponds to an electron density of 8 cm^{-3}. The lines at 50 kHz and 75 kHz correspond to the second and third harmonics of the electron plasma frequency. The fundamental emission intensifies during the interval 1002–1004 UT. Similar observations have been interpreted as being due to electrons reflected upstream by the earth's bow shock [*Filbert and Kellogg*, 1979]. These particular wave intensifications occurred when the interplanetary magnetic field changed direction in such a way as to "connect" the upstream spacecraft with the bow shock. Since this phenomenon also occurs before 0956 UT, it is probably not related to the release experiment. In any case, the Langmuir wave intensifications were not observed during the ECH emissions. The existence of the emissions at the harmonics of the plasma frequency is interpreted by *Cairns and Melrose* [1985] as evidence of a nonlinear mode conversion process of the Langmuir waves in the solar wind. The weak emissions above 50 kHz between the second harmonic and the upper frequency limit of the SFR have not been identified as a product of the lithium release. They may be connected with the terrestrial kilometric radiation observed simultaneously at higher frequencies [*Häusler et al.*, 1986].

Figure 1 shows 30 s of data from the wideband receiver aboard the IRM. The electric field waveform information is transmitted to the ground in two AGC-controlled analog channels: one covering the frequency range 650 Hz to 10 kHz and a second channel for the frequency range 5 Hz to 1 kHz. The top panel of the figure is a spectrogram of the high-frequency channel in the range of 0–2 kHz. The middle panel is a spectrogram of the low-frequency data over the range 0–1 kHz. The bottom panel displays as a function of time the angle between the antenna and the magnetic field. A vague structure of the emissions at intervals of 250 Hz is evident in the top spectrogram. As the antenna becomes perpendicular to the magnetic field, the diffuse noise between the harmonic emissions sometimes disappeared, leaving only a set of narrow-band harmonics in the top panel. This effect may be due to the automatic gain control of the receivers reacting to an amplitude change in the emissions. This effect is very pronounced at several times in the figure, for example, at 0958:10.5 UT and again at 0958:21.5 UT. The emission lines in the top spectrogram are within the third, fourth, and fifth harmonic bands. The harmonic bands are somewhat less obvious in the middle panel. When the antenna was perpendicular to the magnetic field, the low-frequency spectrogram generally shows a narrow-band emission at approximately 430 Hz. The higher harmonic band emission at 730 Hz is difficult to see in the low-frequency spectrogram because of the dynamic range of the gray scale. At times when the antenna is most parallel to the magnetic field in the electric field spectrum is significantly different. During most spin cycles a maximum at approximately 200 Hz was observed with an associated tail of noise which extends up to 1 kHz. Additionally, a low-frequency emission was intermittently observed below 100 Hz. An example can

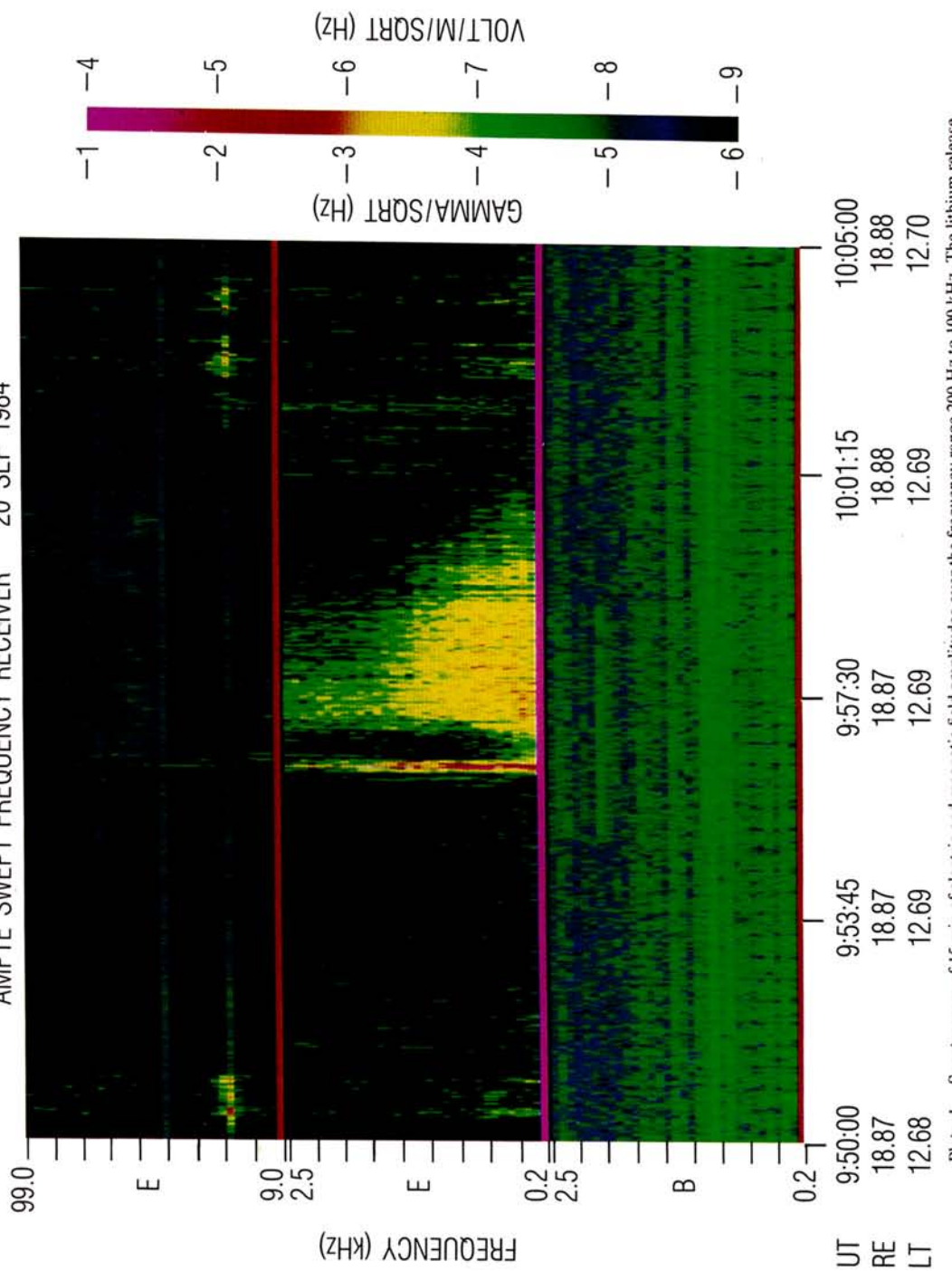

Plate 1. Spectrogram of 15 min of electric and magnetic field amplitudes over the frequency range 200 Hz to 100 kHz. The lithium release occurred at 0956:02 UT.

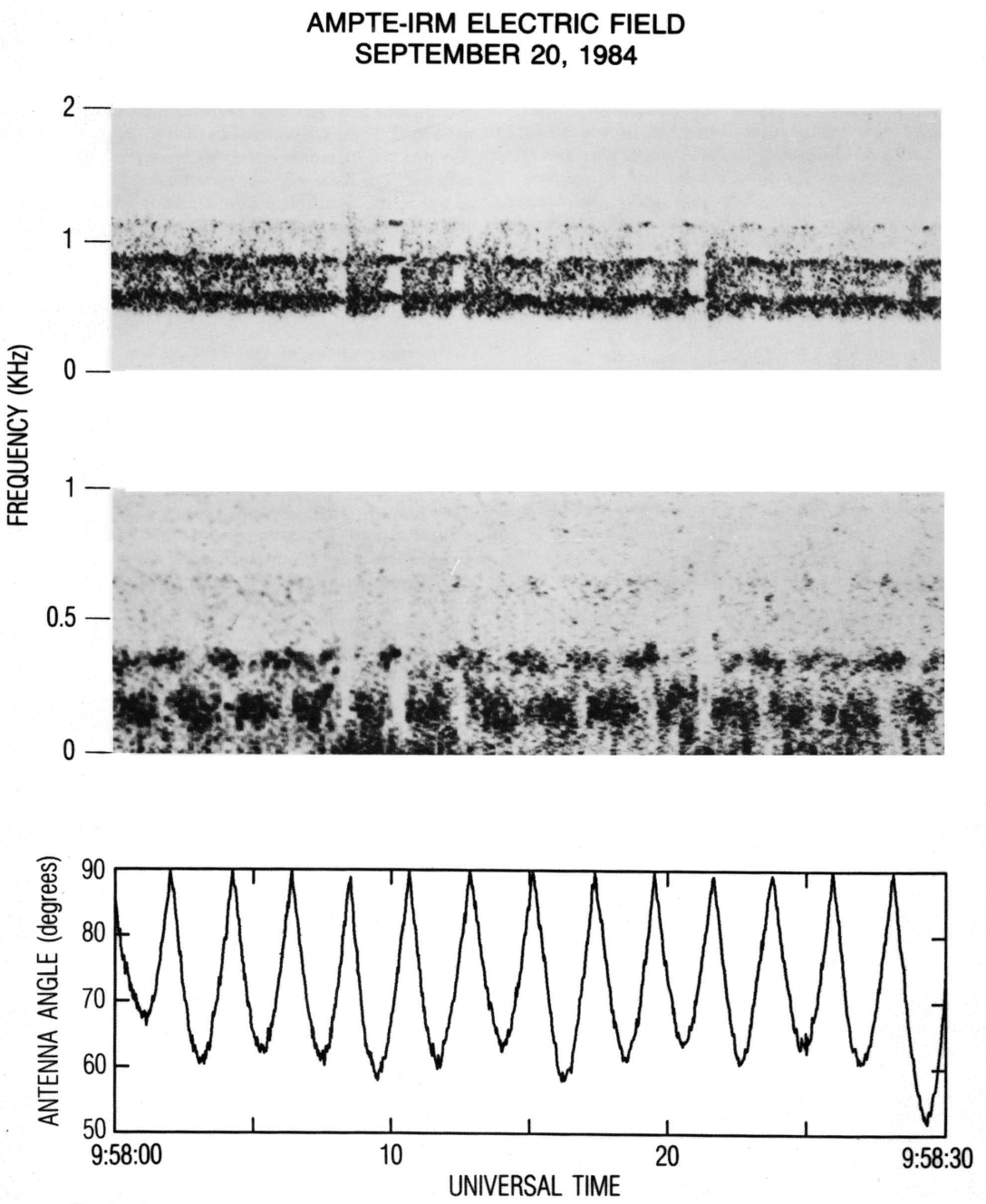

Fig. 1. Spectrograms of 30 s of electric field amplitudes from the two wideband receivers and the antenna spin phase angle.

be seen in Figure 1 in the interval from 0958:06 to 0958:14 UT.

Figure 2 is a composite spectrum of the wideband data during a 0.2-s interval beginning at 0957:50 UT. The antenna was approximately perpendicular to the magnetic field during this interval. The data from the low-frequency receiver are plotted as a solid line, and the high-frequency data are displayed as a dashed line. The amplitude scales of the two receivers have not been intercalibrated. The frequencies of the local electron cyclotron frequency and the first five harmonics are marked by arrows. Narrow-band emissions were observed at 435 Hz, 732 Hz, 1014 Hz, 1292 Hz, and 1566 Hz. These frequencies are 1.8, 3.0, 4.2, 5.3, and 6.4 when normalized to the local electron cyclotron frequency.

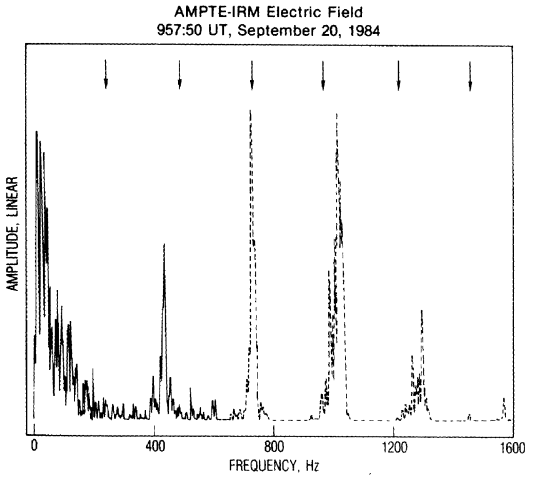

Fig. 2. A composite spectrum of the electric field amplitude during a 0.2-s interval starting at 0957:50 UT. The solid line represents data from the high-frequency channel, and low-frequency data are shown as a dashed line. The frequencies of the local electron cyclotron frequency are marked by arrows at the top of the panel.

The bandwidths of the emissions were very small ($\Delta f/f \sim 0.05$). This value for the bandwidth together with the absolute amplitude information of the SFR imply that each of the narrow-band emissions was of an amplitude of approximately 10^{-5} V m^{-1}. The higher-frequency emissions tended to exhibit the fine structure in their frequency spectrum, as shown in Figure 2. The frequencies and bandwidths of the ECH emissions remained approximately constant throughout the entire period in which they were observed. This spectrum also exhibits the emission below 100 Hz which is mentioned in the discussion of Figure 1.

Figure 3 shows a measurement of the polarization of the emissions with respect to the magnetic field. Two minutes of SFR data was sorted and averaged into three bins on the basis of the angle between the electric dipole antenna and the measured magnetic field. The boundaries of each angular bin are shown at the right of the figure. The angle between the magnetic field and the spacecraft spin vector is 50°–55°, so that the electric field components are measured at angles in the range 60°–90° to the magnetic field. This analysis illustrates that the ECH emissions tend to be polarized in the direction perpendicular to the magnetic field. Superposed on the ECH wave spectrum is a relatively broadband signal of maximum amplitude 6×10^{-7} V m^{-1} Hz$^{-1/2}$. This phenomenon corresponds to the high-frequency tail of the 200-Hz emission seen in the wideband data. The maximum of the spectrum is not observed by the SFR because it is below the lowest frequency channel of the analyzer. The total amplitude of this emission can be crudely estimated by combining the absolute amplitude of the high-frequency tail from the SFR with the relative spectral shape from the wideband data. It is found to be of the order of 10^{-5} V m^{-1}, which is comparable to the amplitude of the ECH emissions. The spin modulation of this signal in the wideband data is not observed in the SFR data, and this modulation may be an artifact of the wideband AGC system.

In summary, the plasma wave instrument on the IRM observed wave emissions during the second AMPTE lithium release into the solar wind. These emissions occurred at times from 50 s to 250 s after injection. They exhibited a cyclotron harmonic frequency structure which was most pronounced at angles near perpendicular to the static magnetic field. These characteristics tend to support the assumption that the harmonic emissions were predominantly electrostatic. The harmonic signature tended to be obscured by an apparently isotropic diffuse emission which ranged from 100 Hz to 1 kHz, with an amplitude maximum sometimes observed at 200 Hz, which was below the cyclotron frequency.

Plasma Observations

The observations of the local plasma population were performed by both the IRM [*Paschmann et al.*, 1986; *Möbius et al.*, 1986] and the UKS [*Hall et al.*, 1986; *Coates et al.*, 1986]. These observations have shown that the release generated a number of effects on the solar wind particles, including both retardation of the solar wind ions and electron heating. However, at times later than 60 s after the injection these processes have essentially stopped. During the observations of the ECH waves the data indicate that the electron distribution was essentially identical with that of the prerelease solar wind. The solar wind electron velocity distribution is well represented by an isotropic distribution with a temperature of 18 eV and a density of 8 cm^{-3} drifting at the solar wind velocity of 460 km/s. This drift was approximately 187 km/s parallel and 420 km/s perpendicular to the magnetic field. The density was in close agreement with the value obtained from the plasma wave data. The good agreement of the two electron density measurements indicates that any additional component of the electrons of energy below 15 eV was very small. This discussion neglects the electrons produced by the lithium ionization reaction. It is assumed that these electrons were continually swept up by the solar wind within an electron cyclotron period, so that the entire electron distribution was drifting at the solar wind velocity. The solar wind proton distribution was also observed by the IRM and UKS instruments during the ECH emissions. It was a nominal solar wind distribution with a density of 8 cm^{-3} and a temperature of 9 eV [*Coates et al.*,

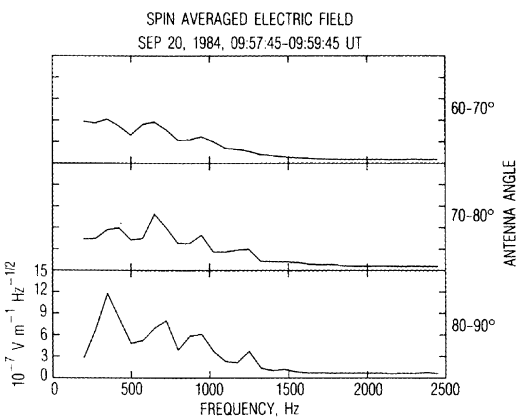

Fig. 3. Average spectrums of the electric emissions observed within each of three bins of the angle between the dipole antenna and the magnetic field.

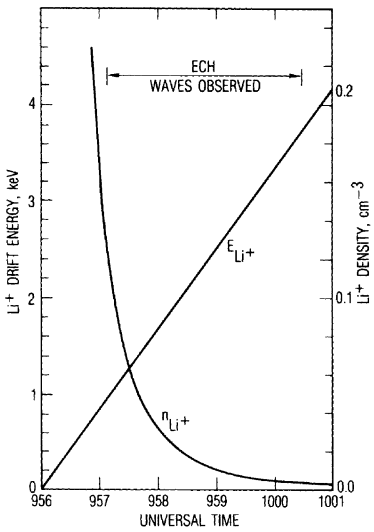

Fig. 4. The number density and drift energy of the lithium ions as a function of time according to a simple release model. The time of observation of the ECH emissions is denoted by the bracket.

1986; *Gurnett et al.*, 1986]. No upstream ion population was observed during the ECH emissions.

The lithium ions generated by the release were observed by two experiments: during the first 100 s by the plasma instrument on the IRM [*Paschmann et al.*, 1986] and by the UKS ion experiment [*Coates et al.*, 1986]. During the second release the time-of-flight ion spectrometer SULEICA on the IRM did not have the proper attitude for lithium observations [*Möbius et al.*, 1986]. A simple model of the release assumes that the neutral lithium cloud took the form of an expanding spherical shell continually ionized by sunlight, producing Li^+ ions at rest with a temperature estimated to be approximately 0.2 eV (G. Haerendel et al., unpublished manuscript, 1985). These ions were then "picked up" or accelerated perpendicular to the interplanetary magnetic field by the solar wind electric field. Since the density of ions was by this time too low to affect the natural fields and plasma, the ions should behave as test particles. The ions traced a cycloidal path perpendicular to the magnetic field. But the radius of lithium shell during the ECH waves was short compared with the lithium cyclotron radius. This means that the ions traveled only a small portion of the cycloid phase and that the lithium velocity distribution was that of a beam in the direction perpendicular to the magnetic field. Figure 4 shows a temporal model of the observed drift energy and density of the ions as extrapolated from Figures 5 and 6 of *Paschmann et al.* [1986]. The drift energies of the ions correspond to drift velocities in the range 166–332 km/s. The time interval in which the ECH waves were detected is marked at the top of the figure. The energy of the ions increases linearly with time, implying a linear increase in the distance over which they have been accelerated by the field. This model of the lithium ion energy is essentially confirmed by the observations during the first 100 s after the release [*Paschmann et al.*, 1986] and at later times [*Coates et al.*, 1986]. The rapidly decreasing density reflects the expanding neutral lithium cloud producing fewer and fewer ions. This density model was derived assuming ionization in a spherically expanding neutral cloud and subsequent acceleration of the ions by a constant electric field (G. Haerendel, unpublished manuscript, 1985). It compares favorably with the data during the first 100 s after the injection [*Paschmann et al.*, 1986]. Comparison with observations at later times is difficult because of the limited ion counting rate, but a similar model was used to interpret high-energy observations of the Li^+ ions in the first release over a time scale of 45 min [*Möbius et al.*, 1986]. The temperature of the lithium beam was below the resolution of the IRM instruments. It can therefore be assumed that this temperature is between the photoionization energy of the lithium and the lower energy threshold of the instruments (0.2–2 eV). Table 2 summarizes the particle observations during the ECH emissions.

Generation Mechanisms

The observed electric field variations seem to be a superposition of several types of wave emissions. One appeared as a diffuse noise with a maximum at approximately 80% of the electron cyclotron frequency. Also present were narrow-band emissions between the harmonics of the electron cyclotron frequency that were polarized perpendicular to the magnetic field.

It is clear from the particle data that the drift velocity of the Li^+ beam relative to the solar wind was a major source, if not the only source, of free energy available in this physical situation. Figure 5 shows the vector geometry involved in the calculation of this parameter. The rectangular coordinate system has been rotated so that the interplanetary magnetic field $\mathbf{B}$ is aligned with the y axis and the solar wind velocity vector $\mathbf{V}_{sw}$ lies in the z-y plane. The angle between the interplanetary magnetic field and the solar wind velocity is denoted by $\theta \sim 66°$. The components of the velocity parallel and perpendicular to $\mathbf{B}$ are shown in the figure as $\mathbf{V}_{sw}^{\parallel}$ and $\mathbf{V}_{sw}^{\perp}$. The solar wind convection electric field is $\mathbf{E}_{sw} = -\mathbf{V}_{sw} \times \mathbf{B}$, and it is directed along the x axis. This electric field accelerates the Li^+ ions, resulting in the lithium ion drift velocity $\mathbf{V}_i$. The difference in velocity between these ions and the solar wind electrons in the electron frame is $\mathbf{V}_{ie} = \mathbf{V}_i - \mathbf{V}_{sw}$. This vector is shown in the figure as perpendicular and parallel components. The parallel component is just the negative of the parallel component of the solar wind velocity, which is nominally 187 km/s. The drift velocities corresponding to the energies of the ions shown in Figure 4 are in the range 166–332 km/s. This gives the perpendicular component of the relative velocity a magnitude in the range 451–535 km/s aligned to the x-z plane.

TABLE 2. Plasma Parameters During the ECH Emissions

Parameter	Value
Solar wind velocity	
Perpendicular, km/s	420
Parallel, km/s	187
Electrons	
Density, cm^{-3}	8
Temperature, eV	18
Protons	
Density, cm^{-3}	8
Temperature, eV	9
Lithium ions	
Density, cm^{-3}	0.03–0.1
Temperature, eV	0.2–2
Drift velocity, km/s	166–332

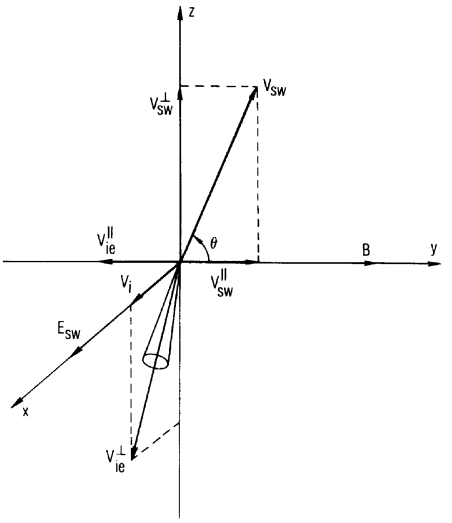

Fig. 5. Schematic diagram of the vector geometry needed to compute the relative velocity of the lithium ions and the solar wind electrons.

The situation of an ion beam streaming through a magnetized plasma at such an oblique angle to the magnetic field rarely occurs in the laboratory or in space. Very little is known about the behavior of such a system under the combined influence of the several applicable instabilities. *Gurnett et al.* [1986] assumed a completely unmagnetized system in the analysis of the intense electrostatic waves observed just after the releases. The later observations of several quite different wave emissions with different polarizations suggest that the magnetic field could have played an important role in their generation. Therefore in this preliminary discussion of instabilities we will try to separate the processes that are driven by the parallel component drift velocity from the ones driven by the perpendicular component.

Several instabilities could be driven by the component of the relative velocity between the Li^+ ions and solar wind plasma which is parallel to the magnetic field. In this case there are three plasma populations which could interact with one another: the solar wind protons, the solar wind electrons, and the Li^+ ions. These are designated in this paper by the letters p, e, and i, respectively. The two processes that are most applicable are the ion acoustic instability [*Fried and Gould*, 1961] and the ion beam plasma instability [*Fried and Wong*, 1966]. The ion acoustic instability could be driven by a relative drift of the solar wind electron and proton components. Normally, the solar wind electron and proton populations both move at the solar wind velocity. But, as outlined by *Gurnett et al.* [1986], the presence of the Li^+ beam could have distorted the solar wind electron distribution via the requirement that the net current be zero. However, during the wave emissions discussed in this work the Li^+ density was so tenuous that the distortion could have been only 1–2 km/s. This distortion was insufficient to destabilize the ion acoustic process for two reasons. First, the relative drift was less than the ion acoustic velocity (45 km/s), which is a critical level for this instability. Second, because $T_e \cong 2T_p$, the ion acoustic waves would have been subject to large amounts of Landau damping by the solar wind protons. So the ion acoustic instability is eliminated as the cause of the observed waves. The ion beam–plasma process could be driven by the relative drift of the proton and Li^+ components. *Gurnett et al.* [1986] cited the ion beam–plasma instability as the cause of the intense burst of electrostatic emissions observed near the upstream edge of the release magnetic cavity. Detailed marginal stability calculations by *Gurnett et al.* [1986] showed that this process requires a lithium to proton density ratio greater than 0.02 to achieve positive growth. This calculation also assumed that the relevant drift velocity was the total solar wind velocity, which was much greater than the parallel component of that velocity. In any case, the range of the density ratio for the duration of the waves under discussion was 0.003–0.0125, so the ion beam–plasma process also appears stable.

Let us now consider the possible role of the perpendicular drift. The electron cyclotron drift or beam-cyclotron instability requires a relative ion-electron drift perpendicular to the magnetic field to amplify electron cyclotron mode waves. If the electron temperature is approximately equal to the ion beam temperature, the wave growth is due to ion Landau damping of the negative energy electron cyclotron mode. This instability has been proposed to generate the electrostatic turbulence observed near the earth's bow shock [*Wu et al.*, 1984]. If the electron temperature is much greater than the ion beam temperature, the instability is caused by the resonant coupling of the negative energy electron cyclotron mode and the Doppler-shifted ion acoustic mode [*Wong*, 1970; *Gary and Sanderson*, 1970]. This is the case which is applicable to the AMPTE release, since the lithium ions were deposited in the solar wind with a temperature that was very low compared to the solar wind electrons. The presence of the solar wind proton population should not have modified significantly the usual characteristics of this instability, because the phase velocity of the electron cyclotron mode was much larger than the average proton velocity, and the wave frequency was much larger than the proton cyclotron frequency. Numerical calculations assuming drifting Maxwellians for the three particle populations show that the system is unstable. However, there is a basic inconsistency between the observations and any proposed electron cyclotron instability process. That is the fact that the only observed electron population was moving at the solar wind velocity. So any electron waves generated by this population would have been Doppler shifted in frequency. The amount and direction of the shift depends on the wave vector. For the minimal shift needed to reproduce the observed emissions the wave vector should be nearly perpendicular to the solar wind velocity. But this is inconsistent with the beam instabilities, which use the relative velocity as a free energy source.

To illustrate this paradox, one may predict by a simple calculation the value of the observed frequency. The wave vector of largest growth rate due to the velocity is parallel to $\mathbf{V}_{ie}^{\perp}$ and set by the Landau resonance of the waves with the Li^+ beam. This is given by

$$\omega = \mathbf{k} \cdot (\mathbf{V}_i - \mathbf{V}_{sw}) \tag{1}$$

where ω is the wave frequency and $\mathbf{k}$ is the wave vector. For the perpendicularly propagating wave mode it can be assumed that $\mathbf{k} \cdot \mathbf{B} = 0$. Since the relative drift velocity is much

less than the electron thermal velocity, electron cyclotron damping should limit the angle of propagation to less than 1° from that perpendicular to **B** [*Wong*, 1970]. The wave frequency observed by the instrument is Doppler shifted according to the usual formula:

$$\omega' = \omega + \mathbf{k} \cdot \mathbf{V}_{sw} = \mathbf{k} \cdot \mathbf{V}_i \tag{2}$$

Elimination of the wave vector from equations (1) and (2) gives a simple relation for the relative Doppler shift of the wave:

$$\frac{\Delta\omega}{\omega} = \frac{\omega' - \omega}{\omega} = -\frac{(V_{sw}^{\perp})^2}{V_i^2 + (V_{sw}^{\perp})^2} \tag{3}$$

Obviously, the Doppler shift is always negative and can be quite large in magnitude. Using the values of the drift velocities in Table 2, the relative Doppler shift takes values in the range of −0.86 to −0.63. The frequencies will be just above the cyclotron harmonics $\omega = n\Omega_{ce}$, where $n = 1, 2, 3, \cdots$, with each unstable band being quite narrow because of the small Li^+ beam temperature. The maximum number of harmonics is limited by the Debye length criterion [*Wong*, 1970]. The wave vector of the unstable waves must be less than the reciprocal of the Debye length. In this case the Debye length of the plasma is very small ($\lambda_D \sim 0.01$ km), so that the number of unstable harmonics is extremely large ($n \sim 25$). Using a cyclotron frequency of 250 Hz, the predicted frequencies of the observed emissions are at integral multiples of 34 Hz. From Figures 1 and 2 it can be seen that there were many structured emissions in the frequency range of 20–150 Hz. However, there was no evidence of a set of closely spaced harmonic emissions such as those predicted by the above calculation. Therefore the cyclotron drift instability is probably not the cause of the ECH emissions.

There are several other plasma microinstabilities which could produce electrostatic wave emissions with an electron cyclotron harmonic structure in the frequency spectrum. The most well known are a class of instabilities that use the free energy of a positive velocity gradient in the electron distribution function perpendicular to the ambient magnetic field. An example of this type is the loss cone instability, which is often cited as the source of ECH emissions in the magnetosphere (for a complete review, see *Kennel and Ashour-Abdalla* [1982]). In this case, however, the plasma observations showed no evidence of any perpendicular anisotropy in the electron distribution. It is possible that the unstable gradients in the distribution were too small to be resolved by the plasma instrument. Instabilities of this type also have the same problem with the Doppler shift of the wave frequency to very low values. Unlike a beam instability these processes generate waves that propagate at all possible phase angles to the magnetic field. The observed frequencies should cover a wide band, smearing any harmonic frequency structure, which is also inconsistent with the data. The additional frequency structure of the higher harmonic emissions in Figure 2 seems very similar to that observed in magnetospheric ECH emissions, which is not predicted by current theories [*Koons and Fennell*, 1984].

CONCLUSION

Two types of electric wave emissions were observed in connection with the second lithium release by the AMPTE-IRM spacecraft into the solar wind. Electron cyclotron harmonic waves were observed to be polarized perpendicular to the static magnetic field. An apparently isotropic emission was observed superposed on the harmonic emissions. The amplitude of each of the emissions was approximately 10^{-5} V m^{-1}. The sensitivity of the magnetic field instrument was insufficient to determine whether the emissions were electrostatic or electromagnetic, but their spectral and polarization characteristics tend to support the assumption that they are electrostatic. The observations of these waves is shown to be inconsistent with their generation by several types of ion beam instabilities. In particular, the observation of narrow-band emissions at intervals of the local electron cyclotron frequency is inconsistent with any known cyclotron instability. All such hypotheses predict a Doppler shift of the wave frequency to values far below the electron cyclotron frequency. The observed plasma parameters were also not sufficient to generate the diffuse noise by either the ion acoustic or the ion beam–plasma instability.

The inconsistency of the theories for the generation of the waves seems to indicate either that the parameters of the observed particle populations are incorrect or that there exists an additional, unobserved population. The models of the Li^+ ion density and temperature seem to be the most probable sources of error in Table 2 which would affect the ion beam–plasma instability. But even radical changes in these quantities would still not solve the problem with the ECH waves. The simplest explanation for the ECH emissions is an electron population that was relatively stationary with respect to the spacecraft. An upstreaming cold electron beam from the earth's bow shock could possibly have accomplished this, but the direction of the interplanetary field seemed to preclude any possibility of connection to the bow shock along magnetic lines of force. The unobserved electrons released by the ionization of the lithium ions is another possible source of a stationary component. There is no known physical mechanism that would keep these electrons from being picked up by the solar wind. However, the evolution of this electron distribution is not well understood, and it was probably not isotropic. Although this component is relatively small and cold, it may have caused enough positive velocity gradient in the electron distribution to produce waves.

The ECH waves were observed only in connection with the second AMPTE lithium release into the solar wind. Although the source of these waves is not understood, we may speculate that the lack of such waves in the first release is due to the difference in the angle between the interplanetary magnetic field and the solar wind velocity. The generation of ECH waves should be related to the relative ion-electron velocity perpendicular to the magnetic field. In the first release this quantity was approximately one third that of the second release. These observations may be evidence of a critical velocity needed for the generation of the electron cyclotron waves.

Acknowledgments. We wish to express our appreciation to our many colleagues who participated in the development, testing, integration, and data reduction for this experiment. In particular, we acknowledge the efforts of K. Gnaiger (KGM), F. Eberl (Max Planck Institute for Extraterrestrial Physics), D. Odem and R. D. Anderson (University of Iowa), and W. B. Harbridge, A. Allard, D. Katsuda, and D. Bax (The Aerospace Corporation). The research at the Aerospace Corporation was supported in part by the Office of

Naval Research, in part by the U.S. Air Force Systems Command's Space Division under contract F04701-85-C-0086, and in part by the National Science Foundation through grant ATM-8313655. The work at the University of Iowa was supported in part by the Office of Naval Research through contract N00014-82-K-0183 and grant N00014-76-C-0016 and by the National Aeronautics and Space Administration through grants NGL-16-001-002 and NGL-16-001-043 and contract NAS5-28701. The research at the University of Washington was supported by the Office of Naval Research through contract N00014-84-K-0160.

The Editor thanks J. F. Drake and J. Etcheto for their assistance in evaluating this paper.

REFERENCES

Bryant, D. A., S. M. Krimigis, and G. Haerendel, Outline of the active magnetospheric particle tracer explorers (AMPTE) mission, *IEEE Trans. Geosci. Remote Sensing*, *GE-23*, 177–181, 1985.

Cairns, I. H., and D. B. Melrose, A theory for $2f_p$ radiation upstream of the earth's bow shock, *J. Geophys. Res.*, *90*, 6637–6640, 1985.

Coates, A. J., A. D. Johnstone, M. F. Smith, and D. J. Rodgers, AMPTE/UKS ion experiment observations of lithium releases in the solar wind, *J. Geophys. Res.*, *91*, 1311–1319, 1986.

Filbert, P. C., and P. J. Kellogg, Electrostatic noise at the plasma frequency beyond the earth's bow shock, *J. Geophys. Res.*, *84*, 1369–1381, 1979.

Fried, B. D., and R. W. Gould, Longitudinal oscillations in a hot plasma, *Phys. Fluids*, *4*, 139–147, 1961.

Fried, B. D., and A. Y. Wong, Stability limits for longitudinal waves in ion beam plasma interaction, *Phys. Fluids*, *9*, 1084–1089, 1966.

Gary, S. P., and J. J. Sanderson, Longitudinal waves in a perpendicular collisionless shock, *J. Plasma Phys.*, *4*, 739–751, 1970.

Gurnett, D. A., T. Z. Ma, R. R. Anderson, O. H. Bauer, G. Haerendel, B. Häusler, G. Paschmann, R. A. Treumann, H. C. Koons, R. Holzworth, and H. Lühr, Analysis and interpretation of the shocklike electrostatic noise associated with the AMPTE solar wind lithium releases, *J. Geophys. Res.*, *91*, 1301–1310, 1986.

Hall, D. S., D. A. Bryant, C. P. Chaloner, R. Bingham, and D. R. Lepine, AMPTE/UKS electron measurements during the lithium releases of September 11 and 20, 1984, *J. Geophys. Res.*, *91*, 1320–1324, 1986.

Häusler, B., R. R. Anderson, D. A. Gurnett, H. C. Koons, R. H. Holzworth, O. H. Bauer, R. A. Treumann, K. Gnaiger, D. Odem, W. B. Harbridge, and F. Eberl, The plasma wave instrument on board the AMPTE IRM satellite, *IEEE Trans. Geosci. Remote Sensing*, *GE-23*, 267–273, 1985.

Häusler, B., L. J. Woolliscroft, R. R. Anderson, D. A. Gurnett, R. H. Holzworth, H. C. Koons, O. H. Bauer, G. Haerendel, R. A. Treumann, P. J. Christiansen, A. G. Darbyshire, M. P. Gough, S. R. Jones, A. J. Norris, H. Lühr, and N. Klöcker, Plasma waves observed by the IRM and UKS spacecraft during the AMPTE solar wind lithium releases: Overview, *J. Geophys. Res.*, *91*, 1283–1299, 1986.

Kennel, C. F., and M. Ashour-Abdalla, Electrostatic waves and the strong diffusion of magnetospheric electrons, in *Magnetospheric Plasma Physics*, edited by A. Nishida, pp. 245–344, Center for Academic Publications, Tokyo, Japan, 1982.

Koons, H. C., and J. F. Fennell, Fine structure in electrostatic emission bands between electron gyrofrequency harmonics, *J. Geophys. Res.*, *89*, 3015–3018, 1984.

Krimigis, S. M., G. Haerendel, R. W. McEntire, G. Paschmann, and D. A. Bryant, The Active Particle Tracer Explorers (AMPTE) Program, *Eos Trans. AGU*, *63*, 843–850, 1982.

Lühr, H., D. J. Southwood, N. Klöcker, M. Acuña, B. Häusler, W. A. C. Mier-Jedrzejowicz, R. P. Rijnbeek, and M. Six, In situ magnetic field measurements during AMPTE solar wind Li^+ releases, *J. Geophys. Res.*, *91*, 1261–1270, 1986.

Möbius, E., D. Hovestadt, B. Klecker, M. Scholer, G. Gloeckler, F. M. Ipavich, and H. Lühr, Observation of lithium pickup ions in the 5- to 20-keV energy range following the AMPTE solar wind releases, *J. Geophys. Res.*, *91*, 1325–1332, 1986.

Paschmann, G., C. W. Carlson, W. Baumjohann, H. Loidl, D. W. Curtis, N. Sckopke, and G. Haerendel, Plasma observations on AMPTE/IRM during the lithium releases in the solar wind, *J. Geophys. Res.*, *91*, 1271–1281, 1986.

Wong, H. V., Electrostatic electron-ion streaming instability, *Phys. Fluids*, *13*, 757–760, 1970.

Wu, C. S., Y. M. Zhou, S. T. Tsai, P. Rodriguez, M. Tanaka, K. Papadopoulos, K. Akimoto, C. S. Lin, M. M. Leroy, and C. C. Goodrich, Microinstabilities associated with a high mach number, perpendicular shock, *Space Sci. Rev.*, *37*, 63–109, 1984.

R. R. Anderson and D. A. Gurnett, Department of Physics and Astronomy, University of Iowa, Iowa City, IA 52242.

O. H. Bauer, G. Haerendel, B. Häusler, and R. Treumann, Max Planck Institute for Physics and Astrophysics, Institute for Extraterrestrial Physics, 8046 Garching by Munich, Federal Republic of Germany.

R. H. Holzworth, Space Sciences Division, University of Washington, Seattle, WA 98195.

H. C. Koons and J. L. Roeder, Space Sciences Laboratory, The Aerospace Corporation, P. O. Box 92957, Los Angeles, CA 90009

(Received January 8, 1986;
revised October 22, 1986;
accepted October 23, 1986.)